Nuclear Instruments and Methods in Physics Research A 1061 (2024) 169142

Contents lists available at ScienceDirect

Nuclear Inst. and Methods in Physics Research, A

journal homepage: www.elsevier.com/locate/nima

Technical Notes

Non-negative sparse deconvolution method for PMT signals in radiation detectors

Tiago M. Quirino [a,b,*], Luciano M. de Andrade Filho [a]

[a] Federal University of Juiz de Fora, Galpão Engenharia Elétrica - Via Local, Juiz de Fora, 36036-900, Minas Gerais, Brazil
[b] Rio de Janeiro State University, R. São Francisco Xavier, 524l, Rio de Janeiro, 20550-013, Rio de Janeiro, Brazil

ARTICLE INFO

Keywords:
Deconvolution
Sparsity
Radiation detectors

ABSTRACT

The electrical signals generated by radiation detectors are often subject to undesired effects that can affect the energy resolution of the detector. These effects may be caused by the measurement system itself or by the high rate of events. Traditional methods for shaping the signals and mitigating these effects often have limitations, such as requiring explicit information about the signals. In this paper, the authors propose a deconvolution method based on least square filtering and non-negative sparsity theory to address these limitations. The method is evaluated using simulated data representing a gamma ray detector with a NaI(Tl) crystal and a photomultiplier tube (PMT). The electrical pulses in this system are pre-processed using a CR coupling circuit and a RC integrator. The energy resolution obtained with the traditional method was 6.60%, while the proposed method resulted in an energy resolution of 5.65%. In addition to improving accuracy, the proposed method also reduces implementation complexity.

1. Introduction

Scintillation detectors typically estimate the energy spectrum using photomultiplier tubes (PMTs), which are commonly used as effective detecting devices [1]. PMTs have high sensitivity to light and generate electrical pulses in response to the detection of radiation. The waveform of these signals contains important information for discriminating between different types of light [2]. Flashes of light received by PMTs generate electrical pulses with typically short rise and fall times, so the order of pulse duration is of few nanoseconds [3]. Electronic readout systems are used to process and analyze these signals, applying signal conditioning techniques and correcting for noise and distortions in the measurements [4,5]. This study aims to precisely estimate signal peaks in certain detector applications, providing vital data on deposited energy, using a streamlined digital processing method. This includes energy reconstruction in the particle identification process using calorimeters [6,7], as well as determining the identity, purity, and quantity of radionuclides in specific samples using gamma-ray detectors [8], among other applications.

Traditionally, signal conditioning has been achieved through the use of analog filters and amplifiers. These components shape the signal to adjust the dynamic range of the PMT pulse to the frequency band and amplitude level limits of the measurement system. One common type of analog shaper circuit is the semi-Gaussian (CR-RC^n), which is composed of a differentiation mesh (CR) followed by n integration meshes (RC) [9]. An example of PMT Analog Pulse Processing is a solution presented by Gallin et al. [10] in the RICH detector, of the AMS high energy particle experiment. A shaper circuit CR - RC^5 is used to widen the pulse enough to allow the peak value of the pulse to be measured using the Time Over Threshold technique.

Digital pulse processing techniques allow the synthesis of any weighting function to perform filtering, with any desired pulse shape constraints, replacing fully analog processing [5]. To enable easy signal storage and the application of data processing algorithms, the analog signal from the PMT must be digitized using analog-to-digital converters (ADCs). In order for the main information of the PMT signal to be acquired, it is necessary to have an adequate ADC sampling rate for the PMT signal's frequency range [11]. Additionally, high sampling rates can help to better distinguish background noise by providing a more accurate representation of the sensor signal. In their work, Di Fuvio et al. [12] used digital processing to integrate the digitized signal directly from the PMT. The goal was to recover the energy deposited in the scintillation detector and to compare the results to the standard analog approach, which uses a CR-RC^5 filter and a charge integration circuit. Sosa et al. [13] also compared analog and digital pulse shape discrimination for distinguishing neutrons and gamma rays from a scintillation detector. In analog analysis a CR-RC^6 filter was used followed by a charge integration circuit, and a high-speed ADC followed by an integration algorithm for the digital analysis. Both

* Corresponding author at: Rio de Janeiro State University, R. São Francisco Xavier, 524l, Rio de Janeiro, 20550-013, Rio de Janeiro, Brazil.
E-mail addresses: tiago.quirino@cern.ch (T.M. Quirino), lucianom@cern.ch (L.M. de Andrade Filho).

https://doi.org/10.1016/j.nima.2024.169142
Received 20 September 2022; Received in revised form 5 January 2024; Accepted 29 January 2024
Available online 3 February 2024
0168-9002/© 2024 Elsevier B.V. All rights reserved.

studies comparing analog and digital methods found that the digital processing improved discrimination performance.

Despite the advantages of digital processing, implementing a high-speed ADC for each sensor in applications with many PMTs can increase the cost of the project. As an economical solution for digital processing systems, analog pre-filtering by a shaper filter can be used to limit the signal frequency range and ensure appropriate digitization. This operates as an anti-aliasing filter and allows for a posterior digital deconvolution procedure to recover the amplitude peaks of the observed signal, which are characterized by a series of discrete impulses. Stein et al. [14] proposed a deconvolution approach by developing the move window deconvolution algorithm. This algorithm aims to correct amplitude variations induced by the sensor and readout circuit. Jordanov et al. [15] also developed a digital deconvolution algorithm to estimate the energy deposited in a detector by recovering the pulse amplitude from an exponential signal provided by the detector. However, both of these deconvolution methods produced poor signal-to-noise ratios, leading to the use of the more established trapezoidal shaper algorithm [2]. The signal deconvolution approach has been extended in other works. For example, Födisch et al. [16] utilized a high-order IIR (infinite impulse response) filter to deconvolve an exponential signal into a step function. In another study, Zeng et al. [17] employed preliminary digital deconvolution followed by signal amplitude recovery using the trapezoidal shaper algorithm. They initially used an *RC* circuit to broaden the pulse width and reduce the signal bandwidth for digitizing the signal with a low-cost ADC.

The peak amplitude recovery using the trapezoidal shaper algorithm is useful when it is possible to separate the time constants that make up the signal provided by the detector readout circuit. However, this technique requires precise calibration of the parameters defined for the algorithm. The recursion of the shaper algorithm, as characterized in IIR filters, can be a drawback for implementing the method, considering the possibility of using FIR (finite impulse response) filters instead [18].

Alternative deconvolution algorithms based on FIR filters have been proposed to address the effects of peak amplitude variation. For example, the deconvolution matrix can be developed from the inverse model of a detector with a high pileup rate [19] or the least square algorithm can be used to design a deconvolution filter in a similar context [20]. However, deconvolution algorithms based on linear filters often produce artifacts in the estimated signal, such as high-frequency noise amplification, because they are typically high-pass filters in the frequency domain. To solve this problem, new deconvolution algorithms based on the theory of sparse data representation have gained popularity. These techniques are well-suited to the deconvolution process in question, as the truth energy deposition can be interpreted as an impulsive signal and is therefore the sparsest representation of the data that maintains peak amplitude information. Some of the most common sparsity techniques for this context include the greedy Matching-Pursuit (MP), Orthogonal-Matching-Pursuit (OMP), Least-Squares Orthogonal-Matching-Pursuit (LS-OMP), and others [21]. Currently, the Iterative-Shrinkage Algorithms family has gained prominence in signal deconvolution. It has been widely applied in particle detectors in high energy physics [22,23], gamma spectrometry [24], and nuclear medicine [25] due to its efficiency in denoising artifacts and extracting edges while maintaining computational simplicity.

This work proposes the use of a deconvolution method based on the least square estimation algorithm [26] and sparsity theory [21] to recover energy deposition in the signals generated by a radiation detector's readout system. The proposed method is compared to the traditional trapezoidal method and is shown to have better resolution and lower computational cost. To evaluate the performance of the proposed method, a simulated dataset is used, that includes the amplitude variation effects, which signifies a challenging for energy recovery. The results of the comparison demonstrated that the proposed method was more efficient in scintillator detectors.

In the second section of this work, the pulse modeling procedure and the effects that characterize the radiation detection problem are presented. The following section describes the deconvolution methods and their mathematical development. The results section includes a discussion of the simulated dataset, the parametric search for the algorithms, and the comparison between the methods, which demonstrates the superiority of the proposed algorithm.

2. Pulse modeling

The waveform model designed by the analysis of the data acquisition system in scintillating detectors may be described using the concept of modular design. Fig. 1 shows a block diagram of the typical modules of the readout electronics. This model is useful because it can be interpreted as a convolutional model and allows for the concentration of the dynamic characteristics of all modules into the pulse characteristic of the readout system.

The first module characterizes the electrical signal produced by the sensor that converts the scintillation light in electric current. Scintillators used for gamma-ray spectroscopy typically employ NaI(Tl) crystals as the sensitive material to convert gamma radiation into flashes of light, which are then coupled to individual photomultiplier tubes (PMTs). When light impinges on the scintillator, the PMT converts the light pulse into an electrical signal [27] that is conditioned by an analog circuit, which is divided into amplification and shaper circuits. The amplification circuit adjusts the signal amplitude levels to be suitable for the analog-to-digital converter (ADC). Meanwhile, the chosen CR-RC shaper circuit extends the electrical signal in time, limiting the signal's frequency band for proper sampling by the ADC.

To simplify, the amplification is considered ideal. Its frequency response and non-linear characteristics were not taken into account. This allows for the normalization of the amplitude in the range $[0, 1]$. Additionally, the ADC quantization error is neglected. Despite these simplifications, the proposed model for scintillating detectors accurately represents the effects of amplitude variation.

2.1. Amplitude variation effect

The amplification carried out by the conditioning circuit is unable to completely mitigate electronic noise, baseline shift, and pileup, leading to amplitude variations that ultimately impair the analysis of the energy spectrum.

Electronic noise is an unwanted signal disturbance generated within the circuit itself. It is usually caused by thermal noise due to variations in the flow of charge carriers in the components and conductors of the electronic circuit. Randomness is a key characteristic of electronic noise [28]. In many cases, electronic noise follows a zero-mean Gaussian probability distribution [5], as the example illustrated in Fig. 2a.

The baseline shift, or undershoot, is a change in the mean value of the electronic signal without the presence of an energy deposition event [5]. It is originated by a coupling capacitor that separates the high voltage, which powers the PMT, from the electronic readout, in the case of grounded cathode configuration. The average voltage of the capacitor must be zero, which leads to the baseline shift. When consecutive pulses occur with intervals between them smaller than the time it takes for the baseline to return to the true zero, the amplitude of the successive signals is reduced [29], as shown in the example in Fig. 2b.

Pileup is a phenomenon that occurs when non-coincident energy depositions overlap within the same acquisition window [2]. This effect can be seen in Fig. 2c. Pileup is a common problem in high-count rate detectors, and it can significantly impact the energy resolution of the detector.

The choice of the time constant for the differentiation and integration stages is important in balancing the effects of baseline shift and

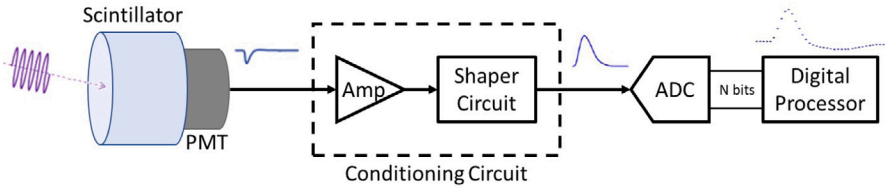

Fig. 1. Block diagram of the readout chain model.

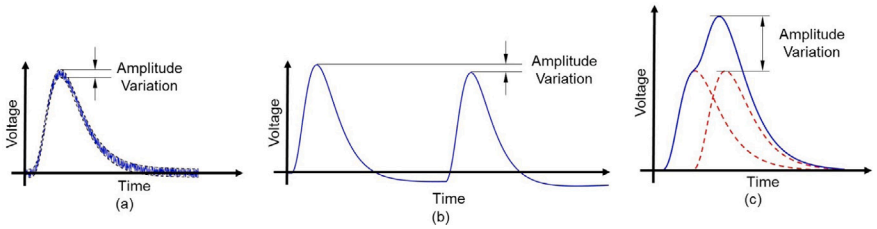

Fig. 2. Main amplitude variation origins from: (a) noise, (b) baseline shift and (c) pile-up.

pileup. Reducing one effect can increase the occurrence of the other, so choosing a time constant equal to the decay time of the NaI(Tl)-PMT set is an optimal point [9].

The coupling capacitor is part of the CR differentiator filter [29]. The pulse duration can be controlled by choosing the time constant of the differentiation stage. A smaller time constant value results in a shorter undershoot duration, accompanied by a larger negative peak and faster pulse decay. This is because the pulse and undershoot areas must be the same. On the other hand, if the capacitance is larger, the undershoot peak is smaller, but the duration is long [2].

The use of RC integrator stages, in analog preprocessing, is also capable of narrowing the pulse width, without modifying the baseline shift, but it increases the signal frequency band, an undesirable effect for digitalization. The signal decay time is one of the main factors to define the pulse width. This is critical in contexts with high event rate, because longer signals in time increase the probability of producing pileup. Therefore, it can be seen that decreasing the decay time, making the pulse narrower, is one of the solutions to prevent pileup, but as mentioned, it can increase the baseline shift.

It is assumed that amplitude variations in the detector measurements should be attenuated through digital processing, as analog preprocessing strategies have not proven to be as effective. Therefore, in this work, algorithms for digital processing are proposed in a dataset influenced by amplitude variations caused by electronic noise, baseline shift, and pileup.

2.2. Convolutional model

The perspective of the radioactive detector readout system as a convolutional model is useful because it allows all the dynamic features to be concentrated in a characteristic pulse of the measurement channel $h[k]$, with $0 \leq k \leq L$, where k is discrete time index, and L is the length or duration of the characteristic pulse in the readout channel. This means that the original signal $x[k]$ only represents the peak amplitudes as discrete impulses. The observed signal of the reading system, $y[k]$, is interpreted as the result of the convolution between the original signal and the characteristic pulse, as shown in the flowchart in Fig. 3

It is worth noting that the signals and the system are analyzed discretely in the convolutional model without loss, as they can be evaluated from the perspective of the digital processor as long as the sampling theorem is satisfied [30].

The convolution model can be analyzed from the perspective of a linear system, represented in matrix–vector notation. The input–output relationship of the measurement systems can be described as:

$$\mathbf{y} = \mathbf{H}\mathbf{x} + \boldsymbol{\sigma} \tag{1}$$

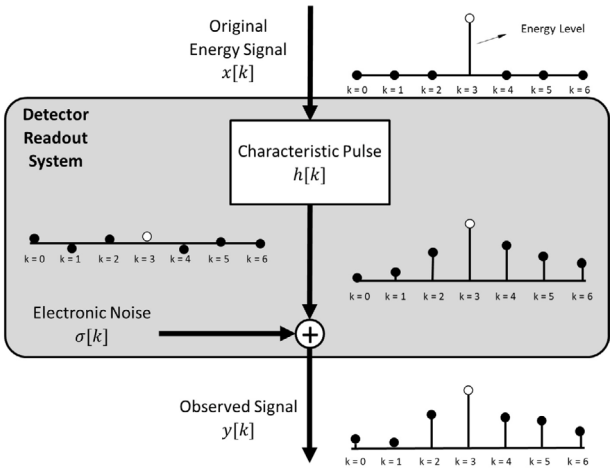

Fig. 3. Convolutional model fluxogram.

where $\mathbf{y} \in \mathbb{R}^K$ is a vector of the observed signal; $\mathbf{x} \in \mathbb{R}^{K-L+1}$ is the original signal to be recovered; and $\boldsymbol{\sigma}$ is the vector of additive noise. $\mathbf{H} \in \mathbb{R}^{K\times(K-L+1)}$ is the convolution matrix where $K > L > 1$. The $K - L + 1$ columns are composed of shifted pulses of $h[k]$ with zero padding. This equation represents a Linear and Time Invariant (LTI) system with a sampling rate that allows us to characterize energy as a weighted Dirac delta function [18].

The goal of using the convolutional model is to simulate the readout system and the original signal in order to create a database of simulated signals and compare different digital peak amplitude recovery algorithms.

3. Digital peak amplitude recovery

Signal peak recovery techniques are used in radioactive detectors because the readout system itself deteriorates the signal, causing variations in the peak amplitudes of the signal [5].

Among the many shaper and/or filtering algorithms, we will discuss the traditional trapezoidal shaper algorithm, which is commonly used in this context, and has been improved by Zeng et al. [17].

3.1. Trapezoidal pulse shape algorithm

Trapezoidal shaping is a common choice for changing the exponential or biexponential pulse shape of the signal provided by the detector

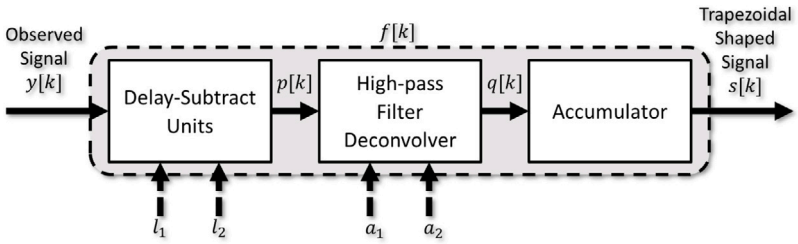

Fig. 4. Trapezoidal shaper algorithm fluxogram.

into a symmetrical flat-top pulse shape. This choice is interesting because it is able to more efficiently handle different decay constants and amplitudes, avoiding the problem of amplitude variations and improving the signal-to-noise ratio [2].

Jordanov et al. developed a recursive algorithm that converts the observed exponential pulse $y[k]$ into a trapezoidal pulse using combined accumulators. To implement this algorithm, parameters must be defined that depend on the application context. The algorithm is defined by the set of equations from their work [31]:

$$u[k] = y[k] - y[k - l_1] \tag{2}$$

$$v[k] = u[k] - u[k - l_2] \tag{3}$$

$$p[k] = p[k - 1] + a_1 \cdot v[k], \quad k \geq 0 \tag{4}$$

$$q[k] = p[k] + a_2 \cdot v[k] \tag{5}$$

$$s[k] = s[k - 1] + q[k], \quad k \geq 0 \tag{6}$$

where l_1 and l_2 are delays that need to be chosen, and the parameters a_1 and a_2 are coefficients that depend on the falling time constant of the exponential decay (τ_f) and the sampling period (T_{clk}), according to the relation:

$$a_1 = \frac{a_2}{e^{T_{clk}/\tau_f} - 1} \tag{7}$$

The trapezoidal shaper operation ($f[k]$) can be divided into stages, as shown in the flowchart in Fig. 4.

In the first stage, two identical operations are performed, according to Eqs. (2) and (3), which are referred to as delay-subtract units by Jordanov. In this stage, the duration of the ascent, descent, and flat part is defined. The duration of flat part, the falling and the rising edges is determined by the value of the delays (l_1, l_2). The operations performed in Eqs. (4) and (5) act as a low-pass filter, called a high-pass filter deconvolver. This also means that the second stage operates as a pole-zero cancellation algorithm, composed of a multiplier–accumulator with coefficient a_2 and a multiplier with coefficient a_1, where the parameter a_2 is able to change the digital gain of the algorithm and the parameter a_1 is defined as a function of the decay time constant of the input signal. The last stage is an accumulator that implements the algorithm, according to Eq. (6) [31].

Zeng et al. [17] noticed that the trapezoidal shaper algorithm was restricted to detectors with bi-exponential pulse characteristics. They therefore proposed a complementary deconvolution algorithm to convert bi-exponential pulses into uni-exponential ones, using the equation:

$$r[k] = y[k] - a_0 \cdot y[k - 1] \tag{8}$$

where the parameter $a_0 = e^{-T_{clk}/\tau_r}$ and τ_r is the rising time constant of the bi-exponential signal. This involves including an additional stage, which can be interpreted as a high-pass filter, similar to the delay-subtract units in the original algorithm.

After implementing the complete shaping algorithm, a peak search algorithm is used to estimate the height of the trapezoid, in order to allow comparison with deconvolution methods. The block diagram for the complete peak amplitude recovery algorithm is shown in Fig. 5. The algorithm evaluates whether the central sample is greater than the side samples ($s[k + \frac{l_1+l_2}{2}] < s[k] > s[k - \frac{l_1+l_2}{2}]$) [32], considering that $\frac{l_1+l_2}{2}$ is rounded to the nearest integer. If both comparisons are true, all samples in the evaluated interval are set to zero, with the exception of the central sample, which must be preserved, and the estimated trapezoidal signal is formed $\hat{x}_{II}[k]$.

3.2. Method of least square

Linear filtering algorithms provide an estimated response $\hat{x}[k]$ from a sequence of N consecutive samples $\mathbf{y}[k] = y[k], y[k-1], \ldots, y[k-N]$ taken from an observed signal $\mathbf{y}$, which are combined linearly with filter weights $\mathbf{w} = w[0], w[1], \ldots, w[N-1]$. The filter order is defined by N, and the algorithm performs a convolution operation:

$$\hat{x}[k] = \sum_{i=0}^{N-1} w[i]y[k - i] \tag{9}$$

In the context of peak amplitude recovery, the filter is required to remove the pulse shape of the readout channel (inverse filter). The inverse filter method relies on a known observed signal pulse shape, which can be obtained through the pulse injection method or by utilizing a reference detector. The efficiency of the estimation in relation to the desired result depends on the adjustment of the filter weights, for which the least squares algorithm is suitable, using the optimization criterion of the sum of squared errors between the estimated signal and the original signal. The cost function presented in Eq. (10) is formed [20], also presented in matrix form:

$$J(\mathbf{w}) = \sum_{i=0}^{M-1} (x[i] - \hat{x}[i])^2 = (\mathbf{x} - \mathbf{Yw})^T(\mathbf{x} - \mathbf{Yw}) \tag{10}$$

$\mathbf{Y} \in \mathbb{R}^{N \times M-N}$ is the observation matrix with N rows, defined by the size of the filter and $M - N$ columns formed by the observed signal samples shifted.

By deriving the cost function with respect to the weights and equating the result to zero, it is possible to isolate the weight values, which can be computed using Eq. (11).

$$\frac{\partial J}{\partial \mathbf{w}} = -2\mathbf{Yx} + 2\mathbf{YY}^T\mathbf{w} = 0$$

$$\mathbf{w} = (\mathbf{YY}^T)^{-1}\mathbf{Yx} \tag{11}$$

where matrix $\mathbf{YY}^T$ must be invertible in order to compute the weights. The term $\mathbf{Y}^+ = (\mathbf{YY}^T)^{-1}\mathbf{Y}$ is known as the pseudoinverse of the observation matrix [33]. The samples of the filtered estimated signal $\hat{x}_0[k]$ are obtained from the following equation:

$$\hat{x}_0[k] = \mathbf{w}^T\mathbf{y}_N[k] \tag{12}$$

The Eq. (11) characterizes the filter parameterization stage. The computed weights are implemented in the filtering stage, according to Eq. (12). Both stages are represented in the flowchart of Fig. 6. The observation matrix $\mathbf{Y}$ and the target vector $\mathbf{x}$ are obtained by simulation, with the imperfection conditions in the original signal. For this, the characteristic pulse must be known, and it can be easily

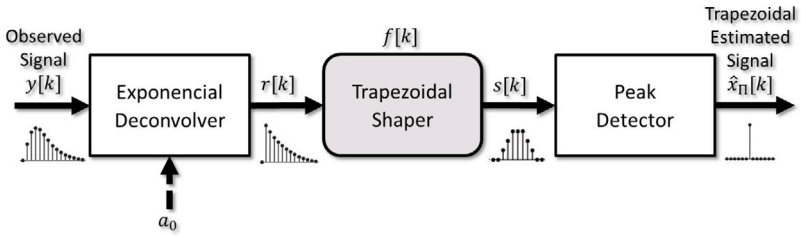

Fig. 5. Complementary trapezoidal shaper algorithm fluxogram.

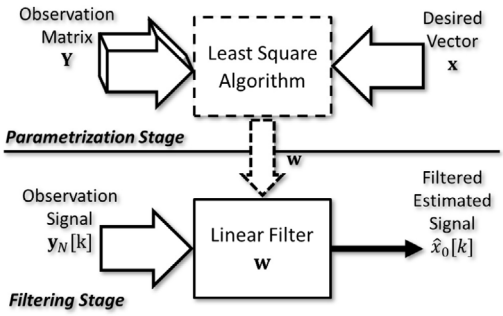

Fig. 6. Least square algorithm fluxogram.

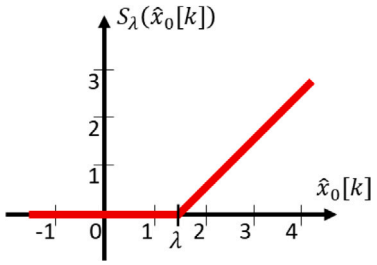

Fig. 7. Example of shrinkage function.

obtained either through electrical simulation of the shaper circuit or experimentally with a precision scope.

By shifting the weights vector to form columns, it is possible to define a weights matrix for deconvolution $\mathbf{W} \in \mathbb{R}^{M\times M}$ and Eq. (9) can be rewrite in matrix form:

$$\hat{\mathbf{x}} = \mathbf{W}\mathbf{y} \tag{13}$$

The disadvantage of the least square filtering algorithm is that it spreads the amplitude level among neighboring samples, as the deconvolution process generates artifacts in samples close to the peak, in addition to amplifying high frequency noise [22].

3.3. Deconvolution by sparsity theory

For PMT amplitude signal recovery, the original digital signal is one with the smallest number of non-zero samples in $\mathbf{x}$, representing the sparsest representation of the data. The theoretical foundation of sparse representations ensures the development of high-performance deconvolution algorithms [21].

Since the signal is embedded in noise, an optimization problem for the sparse representation can be described as [21]:

$$\min_x \|\mathbf{x}\|_1 \ \ subject\ to\ \|\mathbf{x} - \mathbf{W}\mathbf{y}\|_2^2 < \epsilon \tag{14}$$

where the term $\|\mathbf{x}\|_1$ represents the ℓ_1-norm of vector $\mathbf{x}$, which is given by the sum of the absolute values of the coefficients. The minimization of the ℓ_1-norm leads to a sparser representation, but the ℓ_0-norm could also be chosen. The choice of the unit norm is made, as it leads to computationally tractable optimization methods. The term $\|\mathbf{x} - \mathbf{W}\mathbf{y}\|_2^2$ is the ℓ_2-norm square of the deviation between the estimation and the original data, which ensures that the algorithm does not deviate from the model by more than a tolerance value ϵ. The problem is interpreted as an optimization problem through a linear cost function with quadratic constraints [34].

By choosing an appropriate Lagrange multiplier λ [35], the tolerance error ϵ is observed by the λ [23], and this problem can be transformed into an unconstrained optimization problem, according to the cost function given by the equation:

$$J(\mathbf{x}) = \lambda\|\mathbf{x}\|_1 + \|\mathbf{x} - \mathbf{W}\mathbf{y}\|_2^2 \tag{15}$$

the first term, with the presence of the ℓ_1-norm, represents the search for sparsity, while the second, with the ℓ_2-norm, preserves the integrity of the model. The Lagrange multiplier has the role of balancing between the two terms of the expression and need to be obtained experimentally.

In order to minimize the cost function, it should be noted that only non-negative values of the target vector are allowed in this application. Therefore, the modulus operation can be neglected. The above cost function is derived and set equal to zero, from which the equation obtained is:

$$\mathbf{x} = \mathbf{W}\mathbf{y} - \lambda\mathbf{1},\ \mathbf{x} > 0 \tag{16}$$

By decoupling the individual components of the expressions contained in Eq. (16), it is obtained:

$$\hat{x}_\lambda[k] = \mathbf{w}_k^T\mathbf{y}_N[k] - \lambda \tag{17}$$

where $\mathbf{y}_N$ is a vector with N components of the observed signal, $\mathbf{w}_k$ is the kth row of the deconvolution matrix $\mathbf{W}$, and $\hat{x}_\lambda$ is the sparse estimated signal.

Formally, in the context of sparsity theory, the thresholding or Shrinkage technique is interpreted as a nonlinear function, which maps values smaller in modulus than a constant to zero and "shrinks" values outside this range by subtracting them by the constant λ [36].

As the photon interaction in scintillating detectors is always positive ($x[k] > 0$), the nonlinear function is modified such that only the positive range is considered [37]. Therefore, the nonlinear equation (S_λ) is presented in Eq. (18), and demonstrated in Fig. 7.

$$\hat{x}_\lambda[k] = S_\lambda(\hat{x}_0[k]) = \begin{cases} \hat{x}_0[k] - \lambda, & if\ \hat{x}[k] > \lambda, \\ 0, & if\ \hat{x}[k] \le \lambda \end{cases} \tag{18}$$

The operation in Eq. (17) can be understood as a linear filter that performs deconvolution and provides an estimated signal $\hat{x}_0[k] = \mathbf{w}_k^T\mathbf{y}_N[k]$, followed by conditional thresholding. It is possible to use the same linear filter computed by the least-squares method, as shown in the flowchart in Fig. 6. Then, the proposed shrinkage algorithm is applied to the signal estimated by the filter, as depicted in Fig. 8.

The main advantage of sparse deconvolution is that it resolves the issue of amplitude scattering between the observation components, preventing polarization of the results and leading to improved performance in the estimation process.

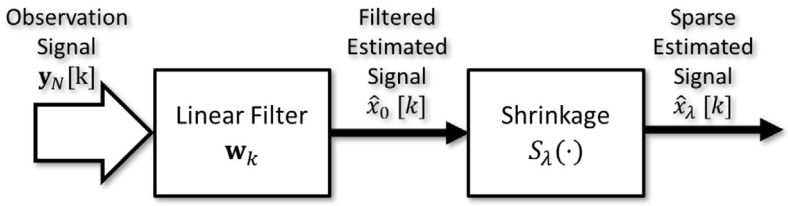

Fig. 8. Proposed sparse filter deconvolution operation.

4. Results

The evaluation of the results is based on the creation of a simulated database and the search for algorithm parameters using the MATLAB software. The performance metric chosen to evaluate the deconvolution, both during the parametric search and in the comparison of methods, is the Root Mean Square of Error (RMSE), calculated using Eq. (19).

$$RMSE = \sqrt{\frac{1}{M}\left(\sum_{i=1}^{M} x[i] - \hat{x}[i]\right)^2} \tag{19}$$

where M is the number of samples.

In the comparison of the results, the Energy Resolution (ER) is also calculated using the FWHM (Full Width at Half Maximum) of the estimated energy spectra and the gamma photo peak at $E_0 = 662$ keV, as shown in Eq. (20) [38].

$$ER = \frac{FWHM}{E_0} \tag{20}$$

4.1. Simulated database

In this work, the typical dominant exponential decay time of the signal from NaI(Tl)-PMT set is considered, which is approximately 230 ns [2], and the time constants of the derivation and integration networks was chosen equal to the decay time of the readout set ($\tau_d = \tau_i = 230$ ns), in order to obtain the best signal-to-noise rate [9]. Using the NI MULTSIM software, a SPICE (Simulation Program with Integrated Circuits Emphasis) simulation was performed of the readout circuit interacting with the electrical signal generated by the NaI(Tl)-PMT set, which defines the characteristic pulse $h[k]$, condensing the dynamic properties of the system.

According to the approximations of the readout circuit, the characteristic pulse can be normalized such that the peak value provides unity gain. However, undershooting cannot be neglected, as shown in Fig. 9.

Due to the choices for the conditioning circuit, the frequency band is reduced to the range from 45 kHz to 7.5 MHz. This allows the conditioned signal to be digitized by an ADC at the minimum rate of 14 MHz, but a frequency of $f_{clk} = 40$ MHz was chosen, similar to what was done in Zeng's work [17] and in the Large Hadron Collider detectors [39].

The signal $x[k]$ can be simulated by selecting two parameters: the scintillation event rate, in order to determine the times of energy deposition, and the energy level spectrum of the interactions in the detector. The energy spectrum data was obtained from a radioactive source of ^{137}Cs reacting with the crystal NaI(Tl), with the photoelectric peak occurring at 662 keV, from the published database provided by Siegel [40]. The average event rate for the database was approximately 40 kcps, but in the simulation, the average event rate was increased to approximately 400 kcps to induce the pile-up effect, according to tests on high count rate system detector efficiency [9]. Using the probability distribution of the energy spectrum and event rate, a Monte Carlo simulator was designed to represent the original signal.

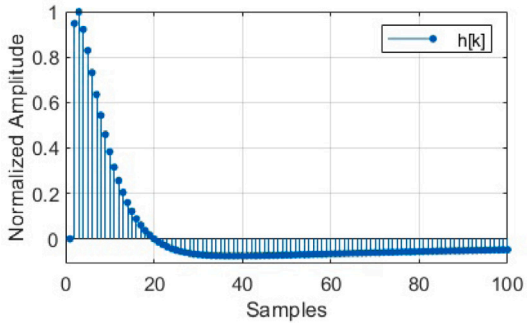

Fig. 9. Characteristic pulse used to create the simulation database.

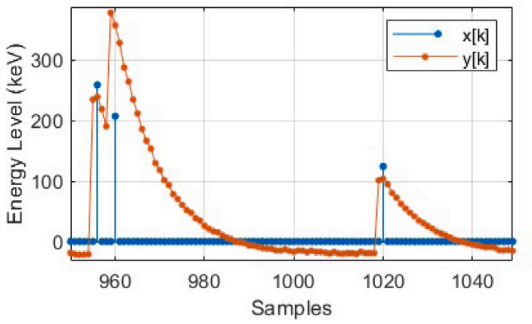

Fig. 10. Portion of original and observed signals in the simulation database.

Based on the convolutional model it is possible to simulate the signal $y[k]$. An example, with part of the observed signal and the original simulated signal, is shown in Fig. 10.

The datasets are then composed of pairs of samples of the input and output signals $\mathcal{T} = (x[k], y[k])_{k=1}^{M}$, where M is the number of samples produced. In order to parameterize the proposed methods, two datasets were formed: a set $\mathcal{U}$ is used for parameterization of the methods, and a set $\mathcal{V}$ is dedicated to efficiency testing and comparison among the methods.

4.2. Parameters selection

The parameterization of all the methods in this work was performed using only the set $\mathcal{U}$, which consists of $M = 10^5$ samples divided into 10 folds to avoid bias in the parameter selection and in the subsequent efficiency comparison.

4.2.1. Trapezoidal shaper algorithm

The trapezoidal shaper algorithm demands the parametric search according to the features of the observed signals. The time constants needed for the coefficient calculations of the observed signal are: $T_{clk} = 25$ ns, $\tau_0 = 10$ ns and $\tau = 230$ ns.

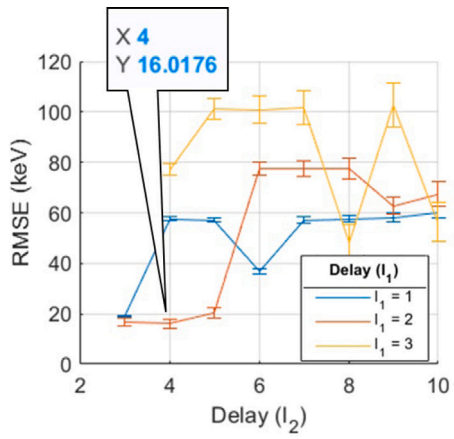

Fig. 11. Interesting error curves for delays variations in trapezoidal shaper algorithm.

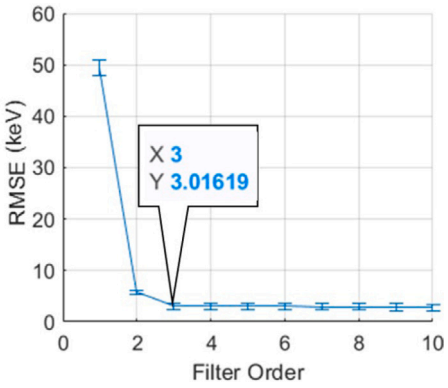

Fig. 12. Filter order error curve.

From the time constants, it is possible to calculate the parameter a_0 directly, while the parameter a_1 depends on the gain a_2, as shown in Eq. (7). The gain was calculated by averaging the ratio between the amplitudes in the original signal and the resulting amplitudes provided by the algorithm. Therefore, the coefficients are: $a_0 = 0.08$, $a_1 = -0.48$ $a_2 = 0.05$.

The choice of delays l_1 and l_2 was performed heuristically, using parameters search that generated a surface error. The 3D representation was not suitable, so a two-dimensional graph was generated from the surface analysis, showed in Fig. 11. As it can be seen, for low delay values the smallest errors are obtained in this context. Therefore, from the analysis of the figure, it was possible to obtain the delay values: $l_1 = 4$ and $l_2 = 2$.

4.2.2. Least square filter

The design of the Least Squares filter algorithm only requires the choice of a parameter, the filter order (N), while the adjustment of the weights depends on the pairs of samples. A new parameterization of the weights is performed for each new filter order and the RMSE is shown in Fig. 12.

As there was no significant improvement with increasing the filter order, the order $N = 3$ was chosen.

4.2.3. Sparse deconvolution

Once the filter order was selected and parameterized, the search for the sparsity parameter is simply a matter of setting the threshold value (λ) of the shrinkage algorithm. Fig. 13 shows the error curve as a function of the threshold value. From the figure, it is possible see that decreasing the parameter returns the result to the least squares filter, while increasing it leads to more sparse representations.

The value of $\lambda = 5$ was found for the threshold.

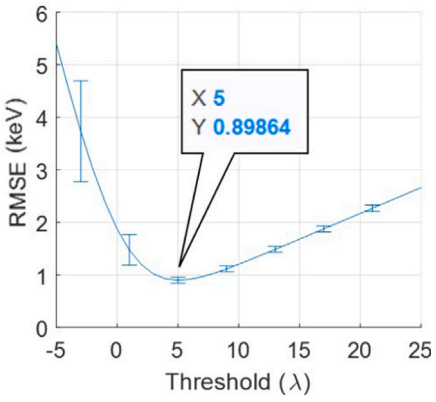

Fig. 13. Threshold error curve.

Table 1
Method performance metrics.

	ER	RMSE
Trapezoidal shaper algorithm	6.60 ± 0.65%	10.71 ± 1.72 keV
Least square filter	5.93 ± 0.53%	3.42 ± 0.09 keV
Sparse deconvolution	5.65 ± 0.50%	1.19 ± 0.03 keV

4.3. Methods comparison

The efficiency of each method is tested using sample pairs in the set $\mathcal{V}$, which consists of $M_{\mathcal{V}} = 10^6$ samples, and that was divided in 5 folds to evaluate the relevance of the comparison. Fig. 14 shows the trapezoidal shaped signal, filtered estimated signal, and sparse filtered estimated signal, along with the reference signal in the same sample range.

Fig. 15 shows the energy spectra obtained from each method. In the low energy range, the method based on sparse theory presents a better reconstruction accuracy.

In addition, Table 1 presents the ER and RMSE for each method. It can be observed that the least squares method improves the energy resolution, which is further improved by the addition of the sparsity perspective.

The RMSE shows that the sparse deconvolution outperforms the trapezoidal method by about 11 times, in addition to outperforming the deconvolution by the least squares method. The improvement achieved by the sparse deconvolution method in ER does not exhibit high significance when compared to the Trapezoidal Shaper Algorithm, mainly due to the spread of the results. However, the Trapezoidal Shaper Algorithm employs three stages whereas sparse deconvolution method is simpler, utilizing only one stage, and still yields superior results.

5. Conclusion

The proposed sparse deconvolution method improves the deconvolution process and recovery of amplitude peaks compared to the traditional shaper algorithm, even in environments with electronic noise, pile-up, and baseline shift. While the least squares filtering method produces results similar to those of the sparsity theory filtering method, the improvement in deconvolution is considerable because it prevents false positives in detecting events with less energy.

While the energy recovery method using the shaper algorithm requires prior knowledge of the parameters corresponding to the readout system, the least squares filtering method using the sparsity theory requires a dataset with pairs of samples for parameterization. From this perspective, the context can be a deciding factor in choosing the energy recovery method. However, when considering the advantages mentioned above, the deconvolution method using sparsity theory is the most interesting.

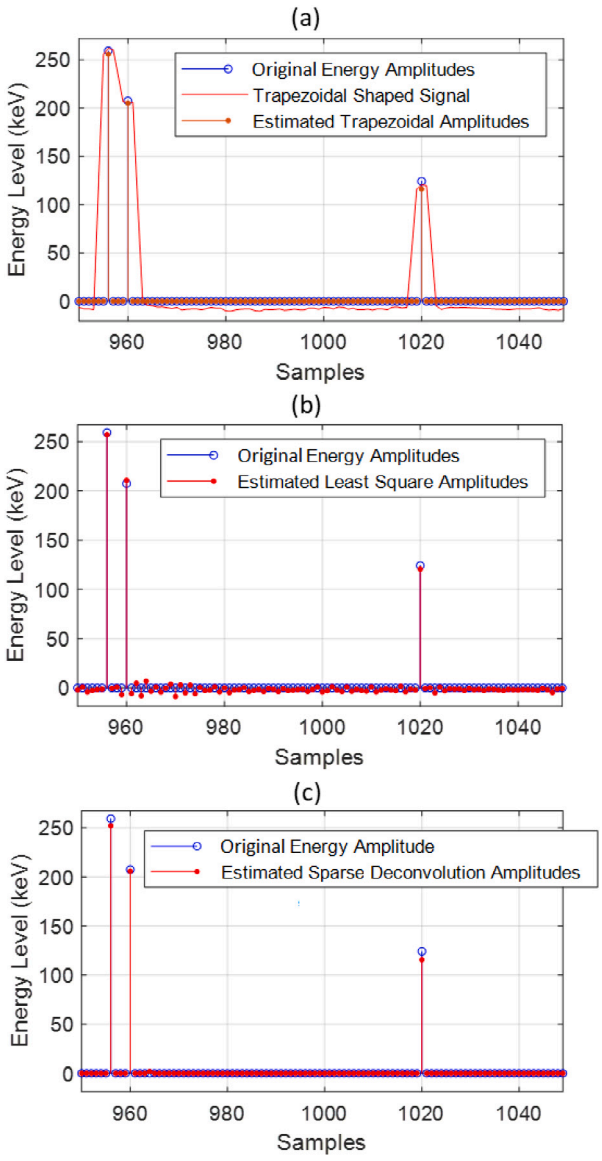

Fig. 14. Samples portion of the same original and estimated signals by: (a) Trapezoidal Shaper Algorithm, (b) Least Square Filter and (c) Sparse Deconvolution.

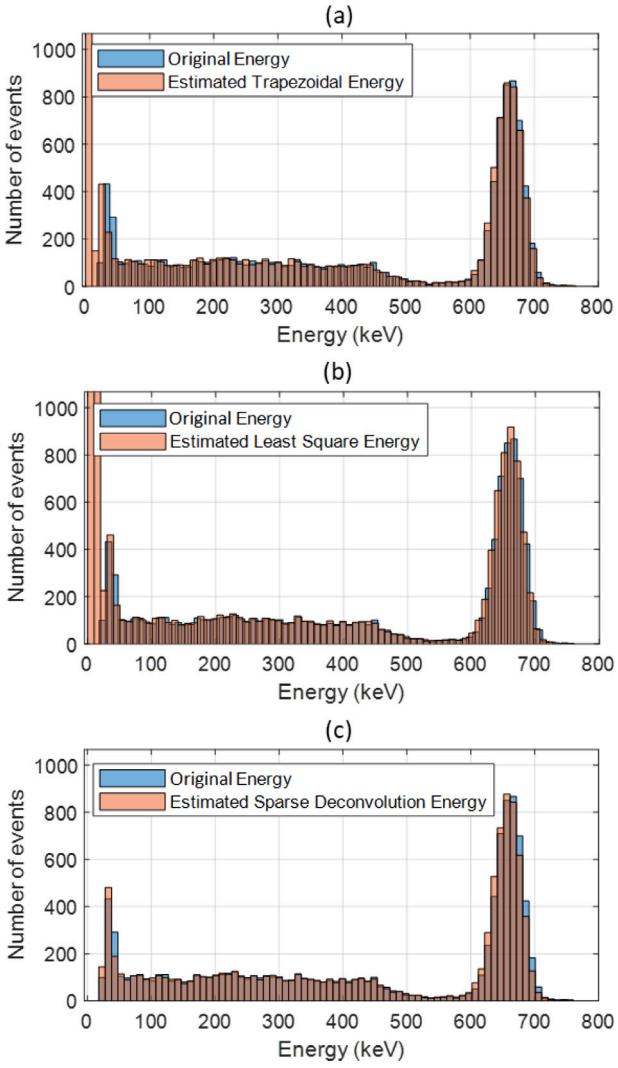

Fig. 15. Energy spectra of estimated and original signal for comparison by: (a) Trapezoidal Shaper Algorithm, (b) Least Square Filter and (c) Sparse Deconvolution.

In addition to the efficiency in recovering peak amplitudes of the signal, we can also compare the complexity of the algorithms. The trapezoidal shaper algorithm is a combination of cascaded filters followed by a peak search algorithm. It uses two FIR filters of order 2 and 4 specifically for the simulated environment in this work, as well as two IIR filters, which, due to the inclusion of feedback in the processing, increase the risk of instability in the peak amplitude recovery system. This is a significant disadvantage as this class of filters can present several implementation problems in fixed point arithmetic. On the other hand, the proposed method reduces the number of operations required to compute peak amplitudes, as it only uses an order 2 FIR filter with no need feedback.

CRediT authorship contribution statement

Tiago M. Quirino: Conceptualization, Investigation, Methodology, Software, Writing – original draft. **Luciano M. de Andrade Filho:** Conceptualization, Formal analysis, Methodology, Project administration, Supervision, Writing – review & editing.

Declaration of competing interest

The authors declare the following financial interests/personal relationships which may be considered as potential competing interests: Luciano Manhaes de Andrade Filho reports a relationship with European Organization for Nuclear Research that includes: employment.

Data availability

Data will be made available on request.

Acknowledgement

The authors would like to thank CAPES, CNPq and FAPEMIG for funding and support for the development of this work.

References

[1] W.R. Leo, Techniques for Nuclear and Particle Physics Experiments: A How-to Approach, Springer Science & Business Media, Berlin, 2012, p. 169.
[2] G.F. Knoll, Radiation Detection and Measurement, John Wiley & Sons, New Jersey, 2010, pp. 234, 292–296, 585–660.
[3] A. Wright, The Photomultiplier Handbook, Oxford University Press, Oxford, 2017, p. 553.

[4] C.S. Draper, W. McKay, S. Lees, Instrument Engineering, vol. 2, McGraw-Hill, 1952.
[5] B. Beckhoff, B. Kanngießer, N. Langhoff, R. Wedell, H. Wolff, Handbook of Practical X-ray Fluorescence Analysis, Springer Science & Business Media, Berlin, 2007, pp. 251–255, 260–261.
[6] C.W. Fabjan, T. Ludlam, Calorimetry in high-energy physics, Annu. Rev. Nucl. Part. Sci. 32 (1) (1982) 335–389.
[7] C. Lippmann, Particle identification, Nucl. Instrum. Methods Phys. Res. A 666 (2012) 148–172.
[8] C.E. Crouthamel, F. Adams, R. Dams, Applied Gamma-Ray Spectrometry, vol. 41, Elsevier, 2013.
[9] H. Spieler, Pulse processing and analysis, in: IEEE Nuclear Science Symposium Short Course, IEEE, San Francisco, 2002, pp. 52–90.
[10] L. Gallin-Martel, J. Pouxe, O. Rossetto, A. Yamouni, A 16 channel analog integrated circuit for PMT pulses processing, in: IEEE Nuclear Science Symposium, IEEE, San Diego, 2001, pp. 742–745.
[11] A.V. Oppenheim, A.S. Willsky, S. Nawab, Signals and Systems: Pearson New International Edition, Pearson Education Limited, Harlow, Essex, England, 2013.
[12] A. Di Fulvio, T. Shin, M. Hamel, S. Pozzi, Digital pulse processing for NaI (Tl) detectors, Nucl. Instrum. Methods Phys. Res. A 806 (2016) 169–174.
[13] C. Sosa, M. Flaska, S. Pozzi, Comparison of analog and digital pulse-shape-discrimination systems, Nucl. Instrum. Methods Phys. Res. A 826 (2016) 72–79.
[14] J. Stein, F. Scheuer, W. Gast, A. Georgiev, X-ray detectors with digitized preamplifiers, Nucl. Instrum. Methods Phys. Res. B 113 (1–4) (1996) 141–145.
[15] V.T. Jordanov, Deconvolution of pulses from a detector-amplifier configuration, Nucl. Instrum. Methods Phys. Res. A 351 (2–3) (1994) 592–594.
[16] P. Födisch, J. Wohsmann, B. Lange, J. Schönherr, W. Enghardt, P. Kaever, Digital high-pass filter deconvolution by means of an infinite impulse response filter, Nucl. Instrum. Methods Phys. Res. A 830 (2016) 484–496.
[17] G.-Q. Zeng, J. Yang, M.-F. Yu, K.-Q. Zhang, Q. Ge, L.-Q. Ge, Digital pulse deconvolution method for current tails of NaI (Tl) detectors, Chin. Phys. C 41 (1) (2017) 016102.
[18] S.K. Mitra, Y. Kuo, Digital Signal Processing: A Computer-Based Approach, vol. 2, McGraw-Hill, New York, 2006, p. 43,73,87.
[19] L.M. de Andrade Filho, B.S. Peralva, J.M. de Seixas, A.S. Cerqueira, Calorimeter response deconvolution for energy estimation in high-luminosity conditions, IEEE Trans. Nucl. Sci. 62 (6) (2015) 3265–3273.
[20] J. Duarte, L.M. de Andrade Filho, E. de Simas Filho, P. Farias, J. de Seixas, Online energy reconstruction for calorimeters under high pile-up conditions using deconvolutional techniques, J. Instrum. 14 (12) (2019) P12017.
[21] M. Elad, Sparse and Redundant Representations: From Theory to Applications in Signal and Image Processing, Springer Science & Business Media, Berlin, 2010, pp. 9, 111–117.
[22] D.P. Barbosa, L.M. de Andrade Filho, B.S. Peralva, A.S. Cerqueira, J.M. de Seixas, Sparse representation for signal reconstruction in calorimeters operating in high luminosity, IEEE Trans. Nucl. Sci. 64 (7) (2017) 1942–1949.
[23] T. Teixeira, L.M. de Andrade Filho, J.M. de Seixas, Sparse deconvolution methods for online energy estimation in calorimeters operating in high luminosity conditions, J. Instrum. 16 (09) (2021) P09008.
[24] T. Trigano, Y. Sepulcre, M. Roitman, U. Aferiat, On nonhomogeneous activity estimation in gamma spectrometry using sparse signal representation, in: 2011 IEEE Statistical Signal Processing Workshop, SSP, IEEE, 2011, pp. 649–652.
[25] C. Zhao, S. Qiao, J. Sun, R. Zhao, W. Wu, Sparsity-based shrinkage approach for practicability improvement of H-LBP-based edge extraction, Nucl. Instrum. Methods Phys. Res. A 825 (2016) 1–5.
[26] S.S. Haykin, Adaptive Filter Theory, third ed., Prentice Hall, New Jersey, 1996, pp. 483–492.
[27] P. Sibczynski, A. Broslawski, A. Gojska, V. Kiptily, S. Korolczuk, R. Kwiatkowski, S. Mianowski, M. Moszyński, J. Rzadkiewicz, L. Swiderski, et al., Characterization of some modern scintillators recommended for use on large fusion facilities in γ-ray spectroscopy and tomographic measurements of γ-emission profiles, Nukleonika 62 (2017).
[28] G. Vasilescu, Electronic Noise and Interfering Signals: Principles and Applications, Springer Science & Business Media, 2005.
[29] G. Gilmore, Practical Gamma-Ray Spectroscopy, John Wiley & Sons, New Jersey, 2008, pp. 71–79.
[30] S.W. Smith, The Scientist and Engineer's Guide to Digital Signal Processing, California Technical Publishing, San Diego, 1997, pp. 40–43, 100.
[31] V.T. Jordanov, G.F. Knoll, A.C. Huber, J.A. Pantazis, Digital techniques for real-time pulse shaping in radiation measurements, Nucl. Instrum. Methods Phys. Res. A 353 (1–3) (1994) 261–264.
[32] T.H. Cormen, C.E. Leiserson, R.L. Rivest, C. Stein, Introduction to Algorithms, MIT Press, Massachusetts, 2022, p. 22.
[33] J.G. Proakis, Digital Signal Processing: Principles Algorithms and Applications, Pearson Education India, Chennai, 2001, p. 715.
[34] I. Selesnick, Sparse regularization via convex analysis, IEEE Trans. Signal Process. 65 (17) (2017) 4481–4494.
[35] M. Kowalski, Sparse regression using mixed norms, Appl. Comput. Harmon. Anal. 27 (3) (2009) 303–324.
[36] D.L. Donoho, De-noising by soft-thresholding, IEEE Trans. Inform. Theory 41 (3) (1995) 613–627.
[37] T. Boas, A. Dutta, X. Li, K.P. Mercier, E. Niderman, Shrinkage function and its applications in matrix approximation, 2016, arXiv preprint arXiv:1601.07600.
[38] N. Demir, Z.N. Kuluöztürk, Determination of energy resolution for a NaI (Tl) detector modeled with FLUKA code, Nucl. Eng. Technol. 53 (11) (2021) 3759–3763.
[39] C. ATLAS, Atlas tile calorimeter: technical design report, Tech. Rep., CERN, 1996.
[40] P. Siegel, Gamma detector data files, 1998, data retrieved from Cal Poly Pomona Physics Department, http://www.siegelsoft.com/nuclear.html.